Research Square

Preprints are preliminary reports that have not undergone peer review.
They should not be considered conclusive, used to inform clinical practice,
or referenced by the media as validated information.

Quantitative method for evaluating nonstandard tissue absorption characteristics using synergetic near-infrared laser thermography and analytical modeling tools

Xin Tan
United States Food and Drug Administration
Sandhya Vasudevan
United States Food and Drug Administration
Ilyas Saytashev
United States Food and Drug Administration
Devashish Shrivastava
United States Food and Drug Administration
Ilko Ilev
Ilko.Ilev@fda.hhs.gov

United States Food and Drug Administration

Article

Keywords:

Posted Date: June 25th, 2026

DOI: https://doi.org/10.21203/rs.3.rs-9696151/v1

License: This work is licensed under a Creative Commons Attribution 4.0 International License.
Read Full License

Additional Declarations: No competing interests reported.

Version of Record: A version of this preprint was published at Scientific Reports on August 20th, 2026.
See the published version at https://doi.org/10.1038/s41598-026-67729-x.

Quantitative method for evaluating nonstandard tissue absorption characteristics using synergetic near-infrared laser thermography and analytical modeling tools

Xin Tan[1], Sandhya Vasudevan[1], Ilyas Saytashev[1], Devashish Shrivastava[2], and Ilko Ilev[1*]

[1]Office of Science and Engineering Laboratories, [2]Office of Product Evaluation and Quality, Center for Devices and Radiological Health, U.S. Food and Drug Administration, Silver Spring, MD 20993, USA

[*]Ilko.Ilev@fda.hhs.gov

Abstract: The field of laser therapeutic and diagnostic devices has a growing need for innovative experimental and analytical tools to support development of standardized methods for evaluating laser safety and performance. Current laser exposure limits in recognized standards apply only to ocular and skin tissues. These limits do not address safe exposure limits for internal tissues beyond eye and skin, referred to here as nonstandard tissues. Furthermore, the lack of comprehensive databases on laser parameters and tissue optical characteristics complicates the development of quantitative methods for assessing photothermal laser-tissue interactions in nonstandard tissues. To address these gaps, we present a novel proof-of-concept quantitative method for evaluating the absorption characteristics of nonstandard mucosal tissue. The proposed synergetic method integrates laser thermography with computational modeling. Using a near-infrared (NIR) thermography system, we evaluated surface temperatures in *ex vivo* porcine tongue mucosal tissues at a therapeutic wavelength of 980 nm and powers ranging from 250 mW to 1 W. The absorption coefficients obtained using the synergetic method (72.75 m^{-1}) closely matched those from the conventional spectrophotometric method (71.57 m^{-1}), with a low percentage difference of 1.6%. The results indicate method's potential to provide accurate and independent evaluation of the absorption characteristics of nonstandard tissues.

1. Introduction

The field of biophotonics technologies and medical devices utilizing non-ionizing laser radiation is rapidly expanding, with advanced developments spanning the full spectrum of biomedical applications, including neurology, cardiology, oncology, gynecology, urology, photobiomodulation therapeutics, dermatology, and dentistry[1-5]. However, concerning the safety and performance evaluation of emerging diagnostic and therapeutic devices in this field, standardized evaluation tools are lacking This gap is particularly evident by the absence of standard maximum permissible exposure (MPE) safety limits for various internal tissues beyond those MPE limits for ocular and skin tissues specified in recognized laser safety standards ANSI Z136.1-2022 and IEC 60825-1:2014[6,7]. While the MPE limits for eye and skin tissues are well established and supported by decades of animal research, safety limits remain undefined for other organs and internal tissues, such as mucosal, brain, kidney, or cardiovascular tissues, which are referred to here as nonstandard tissues[6-8]. Consequently, device evaluations often rely on extrapolation of skin limits or the application of overly conservative ocular limits to define safe operating conditions.

In addition to photochemical and photomechanical effects, most established safety limits and reported cases of laser-induced tissue damage are associated with photothermal laser-tissue interactions in the visible (VIS) and near-infrared (NIR) spectral ranges[2-5]. As photons propagate through tissue and are absorbed by chromophores (e.g., water, hemoglobin, melanin), heat or thermal energy is generated, leading to temperature elevation and potentially reversable and irreversible tissue-damaging effects[9,10]. For quantitative evaluation of laser-induced photothermal tissue effects, both experimental test methods and computational simulation approaches can be employed. Experimental methods encompass laser thermography for assessing laser-induced thermal spread, including measurements of spatial and temporal surface temperature elevations and distributions[10-12]. Computational approaches include solving laser propagation equations to determine laser energy density distributions, applying bioheat transfer models to compute induced heating, and using thermal dose models to predict related tissue damage[13-15]. The computational simulation approach enables prediction of laser-induced tissue temperature elevation and distributions, as well as tissue damage in space and time as a function of specific laser radiation parameters and tissue properties. However, while the laser radiation parameters relevant for computational modeling are generally straightforward to obtain, tissue optical properties—such as absorption and scattering coefficients—are often unavailable in the published literature,

particularly for nonstandard tissues[16-18]. One such nonstandard tissue is tongue mucosal tissue, which is commonly used to investigate laser-induced photothermal safety concerns associated with laser therapeutic procedures[19-22]. Therefore, innovative test methods, along with independent quantitative data, are important to evaluate the absorption characteristics of nonstandard tissues in the NIR spectral range at therapeutic laser wavelengths.

The primary objective of this proof-of-concept study is to present a novel quantitative method for assessing optical absorption characteristics of nonstandard mucosal tissue, based on the integration of NIR laser thermography and computational modeling. The experimental and computational data provided enable the evaluation and prediction of NIR laser-induced tissue temperature elevation and spatial distribution associated with photothermal laser-tissue interactions and related tissue damage. In addition, this study presents an independent set of comparative data on spectrophotometric evaluation of the absorption and scattering characteristics of nonstandard porcine tongue mucosal tissue in the NIR spectral range of 700-1000 nm. Results from both the synergetic laser thermography and computational modeling approach, and the spectrophotometric assessment of the tissue absorption characteristics demonstrated close agreement, with a low percentage difference of 1.6%.

2. Materials and Methods

2.1. Tissue sample collection and preparation

The presented experimental studies were conducted using fresh *ex vivo* porcine tongue mucosal tissue samples harvested from Landrace/Yorkshire swine aged 6-8 months. The porcine tongue samples were harvested on the morning of slaughter from a local licensed abattoir (Wagner Meats Mount Airy Locker Co., Maryland). No live animals were used or euthanized for the purpose of this study. The porcine model was selected due to the close similarities between porcine and human oral mucosa in terms of anatomical, optical and thermal properties, as well as the comparable size of the tongue[19,20]. Porcine mucosal tissue is widely recognized as an effective *ex vivo* model for studying thermal distribution and tissue damage. Porcine tongues were harvested following slaughter at a certified butcher facility. The tongues were transported to the laboratory on ice within 2-3 hours post-slaughter to minimize tissue degradation. Upon arrival at the laboratory, each tongue was kept on ice until the following preparation for laser irradiation and imaging procedures:

1. Each tongue sample was rinsed with saline solution (NERL BB Saline, Thermo Scientific) and trimmed to maintain <15 mm thickness and <15 cm length.
2. The trimmed tongue was placed in a saline bath on a temperature-controlled heated plate (HP-150A-PL2, Auber Instruments) beneath the irradiation/imaging system to maintain physiologically relevant temperature.
3. Fiducial marks were placed on the lateral surface of the tongue using a permanent black ink marker to ensure consistent targeting of the irradiation beam near the marked regions.
4. The established laser irradiation and imaging protocol comprised 90 s of laser irradiation (laser-on), followed by 90 s of thermal cooling (laser-off), for a total thermal imaging acquisition time of 180 s.
5. The post-irradiated tongue was placed in a warm saline bath and, after 30 min, visually inspected for laser-induced lesions and imaged using a digital microscope.

2.2. Spectrophotometric evaluation

Optical characterization of the porcine tongue mucosal tissue samples was performed using a spectrophotometer (LAMBDA 1050 UV/Vis/NIR, Perkin Elmer, Waltham, MA, USA) equipped with a 150 mm diameter integrating sphere. The spectrophotometric measurements were conducted using five porcine tongue mucosal tissue samples. Each tissue sample was trimmed to a thin slice (<2.5 mm) and sandwiched between two glass slides (each of approximately 1 mm thickness), with a drop of saline solution. Transmittance (Fig. 1a) and reflectance (Fig. 1b) spectra were acquired over a wavelength range of 700 nm to 1000 nm in 5 nm increments.

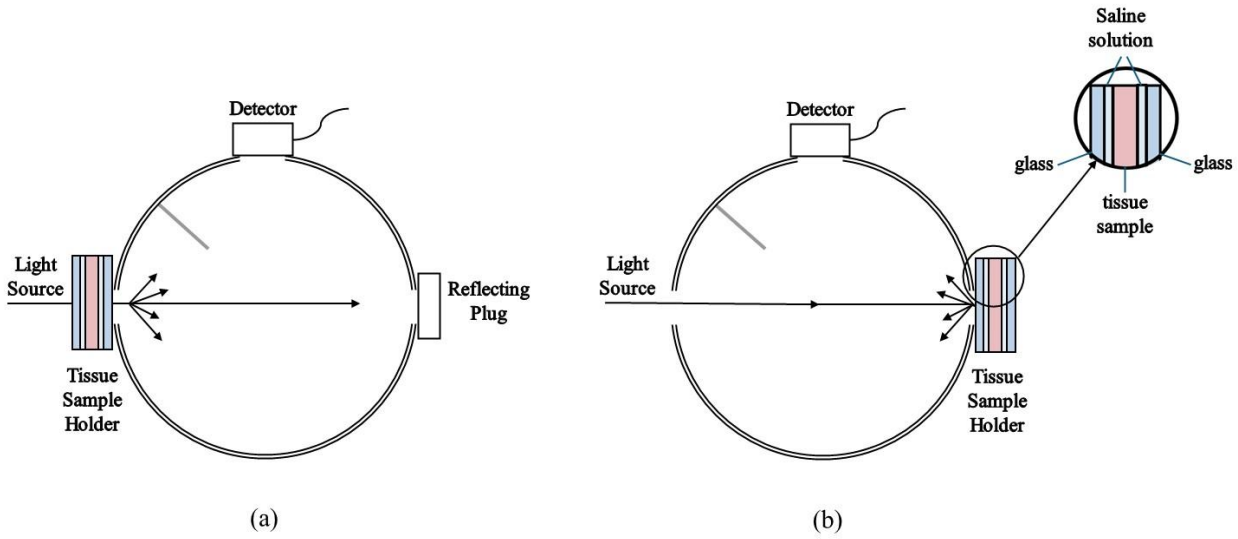


Figure 1. Principal schematic of the spectrophotometric method used for assessing the absorption and reduced scattering coefficients via integrating sphere transmission (a) and reflection (b) measurements of the five-layered sample holder with porcine tongue mucosal tissue samples in the spectral range of 700-1000 nm.

Sphere measurements were calibrated using a Spectralon 99% reflectance standard (Labsphere, Inc., North Sutton, NH, USA). Absorption coefficient (μ_a) and reduced scattering coefficient (μ_s') spectra were obtained using the Inverse Adding-Doubling (IAD) algorithm with a fixed scattering anisotropy factor of 0.9[23]. For each tissue sample, thicknesses were measured at three locations using a digital caliper, and the mean thickness, together with the assumed refractive indices of tissue (n=1.4) and glass slides (n=1.5), was used as input for the IAD algorithm to determine the optical properties across the measured wavelengths.

2.3. NIR laser thermography evaluation

To experimentally evaluate laser-induced thermal spread, including spatial and temporal surface temperature elevations, we designed and implemented a NIR laser thermography setup using an *ex vivo* animal tissue model, as shown in Fig. 1. This multifunctional laser thermography system enables noncontact, noninvasive evaluation of tissue surface temperature distributions and elevations. The test tissue sample is irradiated with a collimated 3.5 mm laser beam at commonly used therapeutic wavelengths such as 808 nm, 850 nm, and 980 nm from fiber-coupled NIR lasers. Irradiation was performed at varying laser radiant power settings ranging from 250 mW to 1 W, with an exposure time of 90 s. The tissue sample is placed in a temperature controlled, half-submerged heating bath to maintain physiologically relevant baseline temperatures.

The NIR laser thermography procedure was implemented on eight ex vivo tongue tissue samples. Six samples were irradiated using various laser radiant power values ranging from 250 mW to 1 W, while two additional samples were used to evaluate the effects of irradiation position, tissue moisture, and high-power exposure. The laser thermography spatiotemporal temperature distributions were measured at 980-nm laser irradiation with six repeated measurements performed at different radiant power levels.

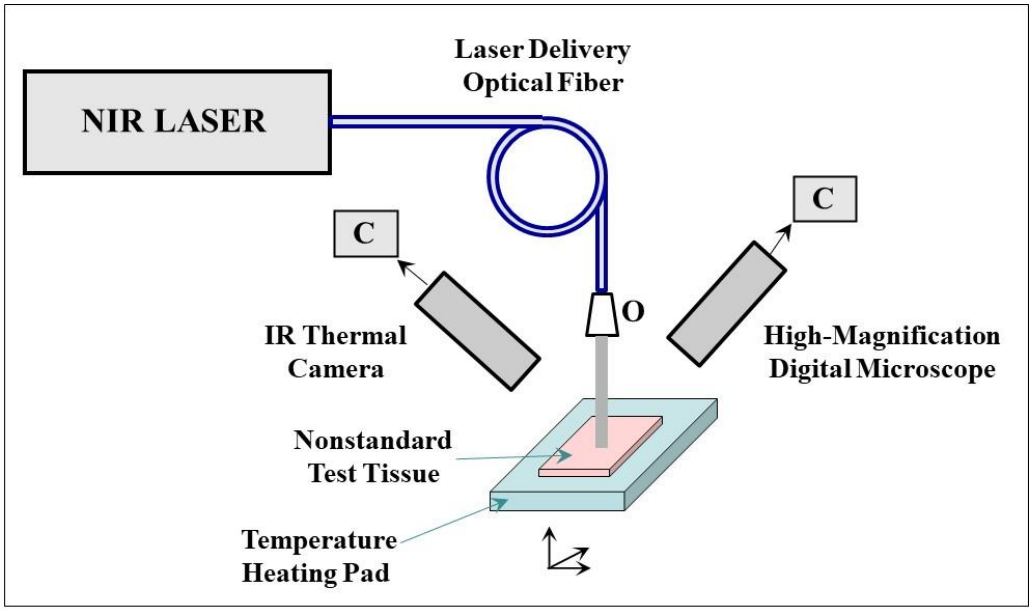


Figure 2. Principle schematic of the multifunctional experimental setup developed for NIR laser thermography evaluation of laser-induced thermal spread and surface temperature elevations using an ex vivo animal tissue model. **NIR Laser**, a CW 808-nm NIR laser; **Laser Delivery Optical Fiber**, a 400-um 0.22-NA laser delivery fiber; **High-Magnification Digital Microscope**, a digital microscope for tissue structural safety evaluation; **IR Thermal Camera**, a high-resolution noninvasive IR thermal camera for temperature measurement and mapping; **Temperature Heating Pad**, a temperature-control heating pad for ex vivo tissue studies, **Nonstandard Test Tissue**, nonstandard porcine tongue mucosal tissue samples; **O**, collimating optics; **C**, computer-controlled data and imaging collection.

Because the operating principle of the developed laser thermography system is based on delivering NIR laser radiation that is absorbed by the tissue sample, the resulting absorption effect leads to localized heat generation and temperature elevation. Laser-induced thermal spread and surface temperature distributions are measured using an IR thermal camera (FLIR A325sc) for thermal imaging along with dedicated application software (ResearchIR4) for thermographic data acquisition. The IR camera provides accurate thermographic imaging (±2ºC or ±2% of reading) and repeatable temperature measurements, with a resolution of 320 × 240 pixels, a high frame rate

(up to 30 Hz for 32-bit), and an instantaneous field of view (IFOV) (or the size of one detector element) of 0.56 mm at a close-focus distance of 18-20 cm. These specifications set the accuracy, precision, and spatial and temporal resolution of the present study. In addition, the experimental setup also includes a digital microscope modality for visual evaluation of laser-induced tissue damage[6-7].

2.4. Computational modeling and simulations

To predict laser-induced tissue temperature distributions in space and time, we solved the relevant equations using COMSOL Multiphysics software. This platform enables efficient implementation of the key coupled laser-tissue photothermal interactions relevant to accurately represent the photothermal processes and heat distribution. We performed COMSOL modeling within a bioheat transfer framework, using parameterization informed by tissue optical measurements. The COMSOL modeling framework considers the diffusion equation (Eq. 1) in conjunction with the *Beer–Lambert* law to describe irradiating beam attenuation and consequent thermal energy deposition and distribution within the tissue (Eq. 2)[10,24-26].

$$\rho \cdot C_p \frac{\partial T}{\partial t} - k\nabla^2 T = Q_{laser} \tag{1}$$

$$Q_{laser} = \mu_{eff} \cdot I_r \cdot exp(-\mu_{eff} \cdot d) \tag{2}$$

Where, ρ $(kg \cdot m^{-3})$, C_p $(J \cdot kg \cdot K^{-1})$, and k $(W \cdot m^{-1} \cdot K^{-1})$ are the density, specific heat, and thermal conductivity of the tissue; Q_{laser} $(W \cdot m^{-3})$ is the heat generation term due to laser-tissue interaction; μ_{eff} (m^{-1}) is the effective attenuation coefficient; and I_r $(W \cdot m^{-2})$ is the laser irradiance. Heat transfer is characterized by the thermo-physical properties of the tissue. Heat generation is determined by the laser parameters and tissue optical properties that are dependent on the laser wavelength.

In COMSOL heat transfer and temperature simulations, the effective attenuation coefficient μ_{eff} generally defines the total energy reduction in a collimated laser beam due to both absorption and scattering effects especially deep in the tissue. However, under the specific experimental conditions considered in this study, laser-induced surface temperature elevation is

defined primarily by absorption of the NIR laser radiation. Surface temperature elevation and two-dimensional temperature distribution are measured using an IR thermal camera, which detects only thermal emission from the tissue surface. Under these conditions, the absorption coefficient (μ_a) is the dominant parameter determining the rate at which absorbed laser energy is converted into thermal energy at the tissue surface[27]. Although scattering influences light propagation and penetration deep within tissue, μ_a primarily determines the efficiency with which optical energy is transformed into thermal energy at the surface of the targeted nonstandard mucosal tissue, which is less than 500 μm thick[28]. Therefore, we assume that the absorption component of the attenuation coefficient (μ_{eff}) is the principal contributor to surface heat generation, directly affecting the resulting surface temperature elevation and distribution of the observed temperature increase. In the COMSOL simulations, as well as in the comparative experimental spectrophotometric and laser thermography measurements, the absorption coefficient is used to define the tissue optical properties. The combined experimental and simulation results were intended to investigate and validate the primary role of tissue absorption characteristics under the presented experimental conditions. Furthermore, both the experimental and simulation studies incorporate the wavelength dependence of the tissue absorption coefficient.

In addition, to quantitatively identify the fitting curve that best matches the experimental laser thermography data and corresponding tissue attenuation coefficients, we employed curve-fitting metrics based on the sum of squared errors (SSE), also known as the residual sum of squares (RSS). The experimental laser thermography data were used to estimate the SSE/RSS values, defined as the squared residual between the peak temperatures of the simulated curve ($\boldsymbol{T_{i,COMSOL}}$) and those of the experimental reference curve ($\boldsymbol{T_{i,laser}}$) at corresponding time points, as expressed by the equation[29]:

$$\boldsymbol{SSE/RSS} = \sum_{i} (\boldsymbol{T_{i,COMSOL}} - \boldsymbol{T_{i,laser}})^2 \quad (3)$$

3. Results and Discussion

3.1. Spectrophotometric data

Using the spectrophotometric test methodology and the experimental setup (Fig. 1) presented in Section 2.2, we measured the absorption (μ_a) and reduced scattering coefficient (μ_s')

characteristics of five samples of nonstandard *ex vivo* porcine tongue mucosal tissue across the 700-1000 nm spectral range.

Figure 3 shows the spectral distributions of the measured absorption (Fig. 3a) and reduced scattering (Fig. 3b) coefficients in the 700-1000 nm range for five tested samples (S1 to S5) of nonstandard *ex vivo* porcine tongue mucosal tissue. The plots also include averaged curves from the experimental measurements along with standard deviation bars with maximum values of 0.039 cm^{-1} (or 5.6% percentage standard deviation) and 1.39 cm^{-1} (or 11%) for the absorption and scattering coefficient measurements, respectively.

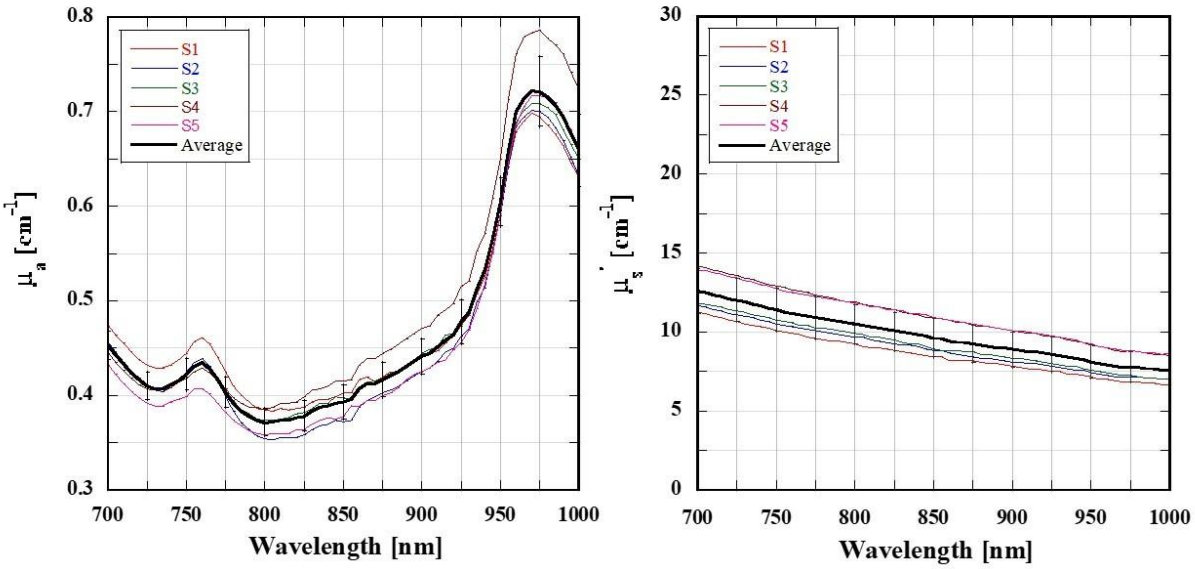


Figure 3. Representative experimental plots from spectrophotometric measurements of the absorption (a) and scattering (b) characteristics of five samples (S1 to S5) of nonstandard ex vivo porcine tongue mucosal tissue. The plots include averaging curves along with error bars indicating standard deviations.

Regarding the spectrophotometric absorption coefficient measurements at the targeted therapeutic NIR laser wavelengths, such as 980 nm, the measured absorption coefficient values along with the average value and standard deviation are listed in Table 1. The average absorption coefficient value obtained from the spectrophotometric data is $\mu_a = 0.7157 \pm 0.036$ $cm^{-1} = 71.57 \pm 3.6$ m^{-1}, corresponding to a percentage standard deviation of 5.0%. These absorption coefficient values are important, as they will be compared to the values evaluated by the laser thermography and computational modeling tools.

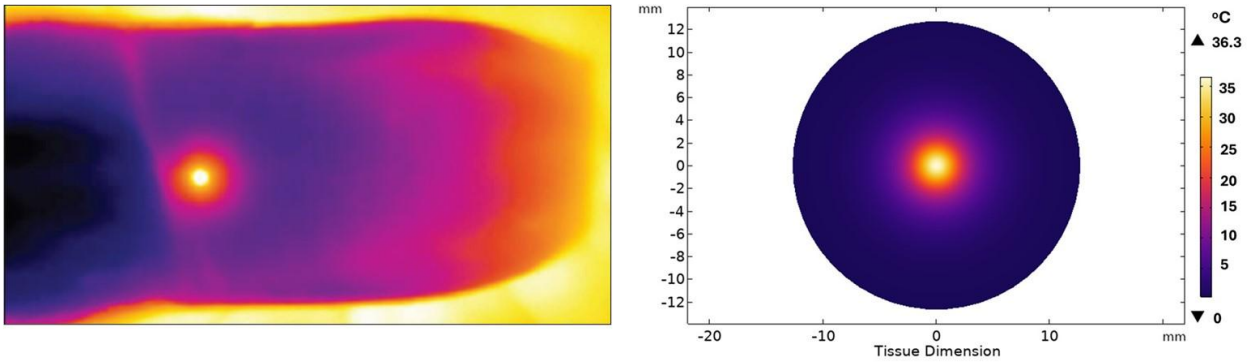
Table 1. Absorption coefficient values [m^{-1}] obtained from the spectrophotometric measurements at a 980 nm laser wavelength, which are tabulated from the data points presented in Figure 3a.

Tissue Sample	S1	S2	S3	S4	S5	Average μ_a [m^{-1}]	STDEV [m^{-1}]
μ_a [m^{-1}]	68.66	69.45	70.42	77.72	71.6	71.57	3.60

3.2. NIR laser thermography and computational simulation data

Applying the NIR laser thermography test methodology and the experimental setup (Fig. 2) described in Section 2.3, we investigated laser-induced photothermal effects and the resulting surface temperature elevation and distributions in porcine tongue mucosal tissue. As a proof-of-concept study for developing and implementing a novel quantitative method to evaluate nonstandard tissue absorption characteristics using laser thermography and computational modeling, we focused on collecting a complete set of experimental data to investigate laser-induced surface temperature elevations and distributions during NIR laser irradiation of the tissue surface at a therapeutic laser wavelength of 980 nm.

NIR laser thermography data were collected to obtained two-dimensional spatiotemporal temperature distributions from *ex vivo* tongue samples under 980-nm laser irradiation at various radiant power levels in the range of 250 mW to 1 W. Thermal imaging movies were recorded at a frame rate of 10 Hz and post-processed in MATLAB to extract peak temperature-time distribution curves over 90 seconds of laser irradiation. Figure 4 shows representative spatiotemporal profiles of the surface temperature distribution measured using NIR laser thermography (Fig. 4a) and the corresponding two-dimensional surface temperature distribution obtained from COMSOL simulations (Fig. 4b).



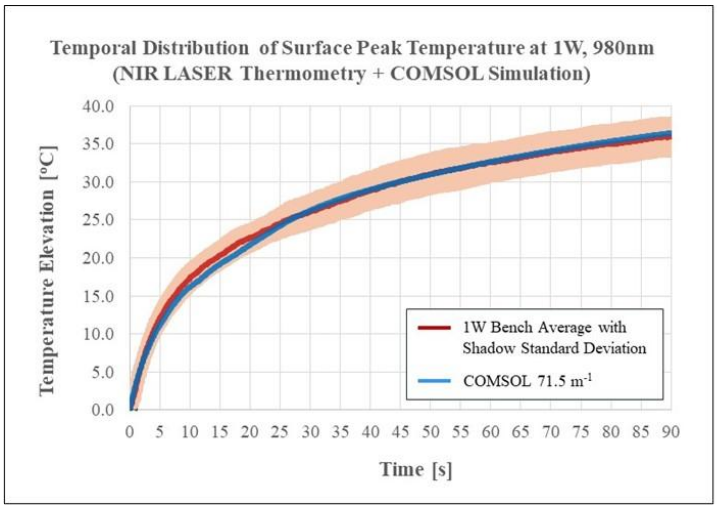
(a) (b)

Figure 4. Representative spatial profiles of the surface peak temperature elevation and distribution measured using the NIR laser thermography (a) and the corresponding two-dimensional surface temperature distribution obtained by the simulations (b) at 980 nm, 1 W laser power and 90 s exposure time.

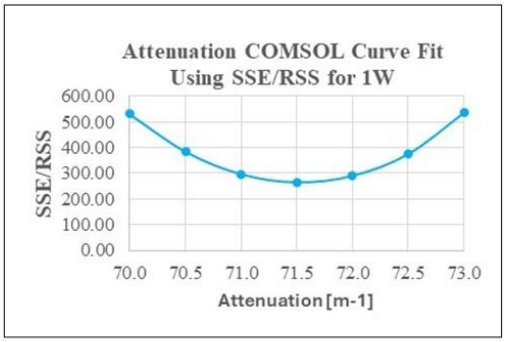
To experimentally evaluate the NIR laser-induced surface temperature elevation and its spatiotemporal distribution in porcine tongue mucosal tissue, we examined the effects of laser radiant power and irradiance using the laser thermography setup. The investigation focused on moderate-to-low laser radiation conditions, including radiant power and irradiance levels below established tissue damage thresholds. Tissue damage was qualitatively assessed at higher power levels using advanced imaging and sensing modalities including digital microscopy. The investigated laser radiant power (and corresponding irradiance) levels were the following: 1 W (10.4 W/cm^2); 750 mW (7.8 W/cm^2); 500 mW (5.2 W/cm^2); and 250 mW (2.6 W/cm^2).

Figure 5 illustrates experimentally evaluated surface peak temperature distributions obtained using NIR laser thermography system along with the corresponding fitted surface temperature distribution from computational simulations. In each figure, the red curve denotes the average experimental measurement with shadow standard deviation and the blue curve represents the simulation result. Both the experimental and computational curves were evaluated at the following laser power levels and tissue attenuation coefficients: a laser power of 1 W and a tissue attenuation coefficient of 71.5 m^{-1} (Fig, 5a); a laser power of 750 mW and a tissue attenuation coefficient of 72 m^{-1} (Fig. 5b); a laser power of 500 mW and a tissue attenuation coefficient of 74.5 m^{-1} (Fig. 5c); and a laser power of 250 mW and a tissue attenuation coefficient of 73 m^{-1} (Fig. 5d). The experimental and computational surface temperature distributions were evaluated at a laser wavelength of 980 nm with an exposure time of 90 s.

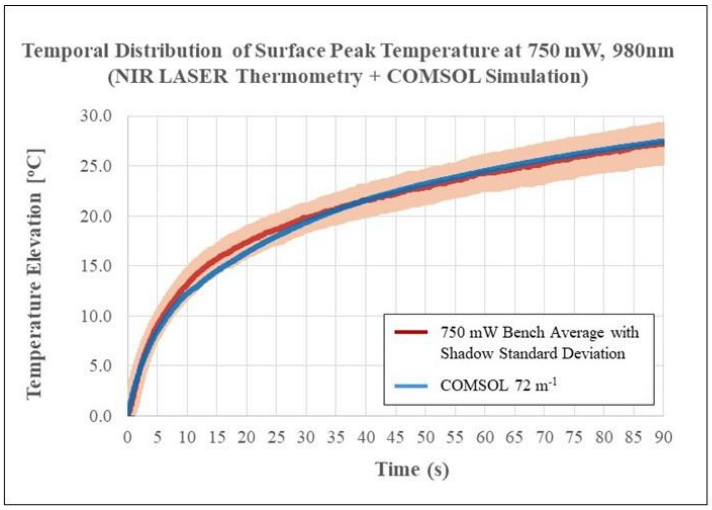
Using the curve-fitting metric approach and Equation 3 defined in the Materials and Methods section, we evaluated attenuation coefficient values with respect to the experimental laser thermography data at the following laser power levels: attenuation coefficient of 71.5 m^{-1} for 1 W power (Fig. 5e); attenuation coefficient of 72 m^{-1} for 750 mW power (Fig. 5f); attenuation coefficient of 74.5 m^{-1} for 500 mW power (Fig. 5g); and attenuation coefficient of 73 m^{-1} for 250 mW power (Fig. 5h).


Temporal Distribution of Surface Peak Temperature at 1W, 980nm
(NIR LASER Thermometry + COMSOL Simulation)
Temperature Elevation [°C]
Time [s]
1W Bench Average with Shadow Standard Deviation
COMSOL 71.5 m-1

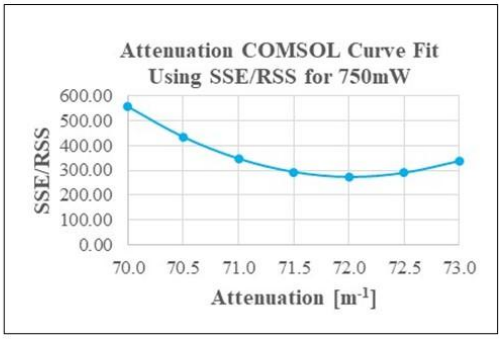
(a)


Attenuation COMSOL Curve Fit
Using SSE/RSS for 1W
SSE/RSS
Attenuation [m-1]

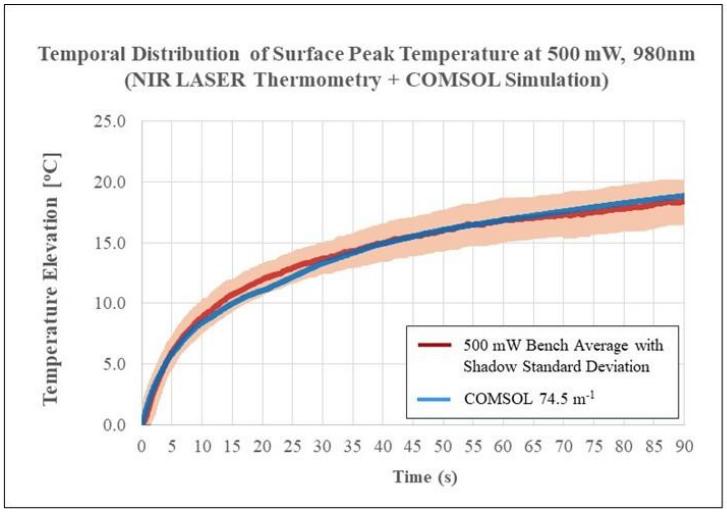
(e)

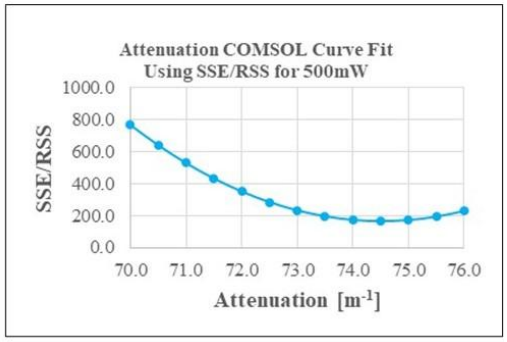

Temporal Distribution of Surface Peak Temperature at 750 mW, 980nm
(NIR LASER Thermometry + COMSOL Simulation)
Temperature Elevation [°C]
Time (s)
750 mW Bench Average with Shadow Standard Deviation
COMSOL 72 m-1

(b)

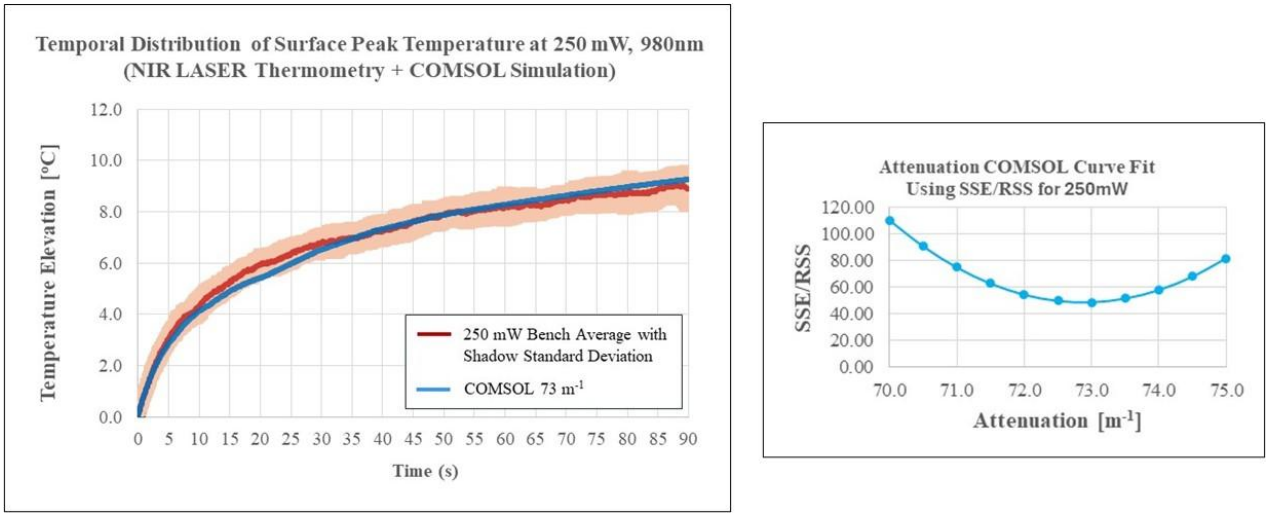

Attenuation COMSOL Curve Fit
Using SSE/RSS for 750mW
SSE/RSS
Attenuation [m-1]

(f)


Temporal Distribution of Surface Peak Temperature at 500 mW, 980nm
(NIR LASER Thermometry + COMSOL Simulation)
Temperature Elevation [°C]
Time (s)
500 mW Bench Average with Shadow Standard Deviation
COMSOL 74.5 m-1


Attenuation COMSOL Curve Fit
Using SSE/RSS for 500mW
SSE/RSS
Attenuation [m-1]

(c) (g)



(d) (h)

Figure 5. Experimentally evaluated surface peak temperature distribution in porcine tongue mucosal tissue obtained using the NIR laser thermography setup along with the corresponding fitted surface temperature distribution from COMSOL simulation at a laser power of 1 W and a tissue attenuation coefficient of 71.5 m^{-1} (a); a laser power of 750 mW and a tissue attenuation coefficient of 72 m^{-1} (b); a laser power of 500 mW and a tissue attenuation coefficient of 74.5 m^{-1} (c); and a laser power of 250 mW and a tissue attenuation coefficient of 73 m^{-1} (d). The best analytical fitting curve and attenuation coefficient were evaluated from the experimental laser thermography data using the sum of squared errors (SSE) or the residual sum of squares (RSS) curve-fitting metric, as the assessed attenuation coefficient values were: 71.5 m^{-1} for 1 W power (e); 72 m^{-1} for 750 mW power (f); 74.5 m^{-1} for 500 mW power (g); and 73 m^{-1} for 250 mW power (h). The experimental and analytical surface temperature distribution data were evaluated at 980 nm laser wavelength and an exposure time of 90 s.

The absorption coefficient values, along with their average and standard deviation obtained using the synergetic NIR laser thermography and computational modeling approach, are summarized in Table 2. As discussed in Section 2.4, these absorption coefficient values correspond to the attenuation coefficient values estimated using the synergetic method under the reported experimental conditions of laser-induced surface temperature elevation. Thus, the average absorption coefficient value is $\mu_a = 72.75 \pm 1.32$ m^{-1}, corresponding to a percentage standard deviation of 1.8%. These results are statistically similar within 95% confidence limits which indicate that the developed synergetic laser thermography and computational modeling approach provides an accurate quantitative method for evaluating the absorption characteristics of nonstandard tissue.

Table 2. Absorption coefficient values [m^{-1}] obtained from the synergetic NIR laser thermography and computational modeling approach developed for investigating nonstandard tissue at NIR laser irradiation.

Laser Power	1 W	750 mW	500 mW	250 mW	**Average μ_a [m^{-1}]**	**STDEV [m^{-1}]**
μ_a [m^{-1}]	71.5	72	74.5	73	72.75	1.32

Furthermore, a comparative analysis of the absorption coefficient values obtained using the proposed synergetic test method (72.75 m^{-1}) and the spectrophotometric method (71.57 m^{-1}) indicated a high degree of agreement, with a low percentage difference of 1.6%. The agreement between these results further demonstrates that the tissue absorption coefficient is the primary contributor to surface heat generation under the reported experimental conditions and thus, it directly affects the resulting surface temperature elevation and distribution. Consequently, these results highlight the potential of the proposed synergetic method to serve as an accurate tool for independently evaluating the absorption characteristics of nonstandard tissues.

4. Conclusion

We have developed and implemented an alternative quantitative method that integrates NIR laser thermography with computational modeling to evaluate the absorption characteristics of nonstandard mucosal tongue tissue. We have demonstrated the applicability of the proposed test methodology for the accurate assessment of tissue absorption coefficients. The assessment capability was verified by independent spectrophotometric measurements of the mucosal tissue. The absorption characteristics data presented here, obtained using both the synergetic laser thermography-thermal modeling method and the spectrophotometric method, contribute to addressing a gap in the literature regarding the absorption coefficients of the tested mucosal tongue tissue. Furthermore, the results have demonstrated the potential of the proposed synergetic method to provide critical input data for surface temperature elevation and distributions from NIR laser thermography as well as absorption coefficients required for computational simulations. These data may be helpful in evaluating NIR laser-tissue photothermal interactions and damage thresholds for specific nonstandard tissues. Moreover, given the expanding use of lasers to diagnose and treat internal organs, the proposed test methodology may be useful in evaluation of other nonstandard tissue types where laser safety limits are lacking.

Acknowledgements

The authors would like to acknowledge constructive discussions with Dr. Daniel X. Hammer and Dr. Joshua Pfefer on photothermal laser-tissue interactions.

The mention of commercial products, their sources, or their use in connection with material reported herein is not to be construed as either an actual or implied endorsement of such products by the U.S. Department of Health and Human Services.

The findings and conclusions in this article are those of the authors and do not necessarily represent any determination or policy of the US Food and Drug Administration.

Author Contributions

X.T. performed NIR laser thermography data collection and processing, and analytical COMSOL simulation; S.V. performed spectrophotometric experiments and data processing; I.S. performed imaging, tissue preparation, and data processing; D.S. provided guidance and feedback throughout the study; I.I. provided experimental setups, guidance and feedback for the experimental and analytical studies, and wrote the initial draft of this manuscript. All authors edited and reviewed the manuscript.

Funding

This study received no external funding from organizations outside the U.S. Food and Drug Administration.

Competing Interests

The authors declare no competing financial interests.

Data Availability

All data generated or analyzed during this study are included in this published article.

References

1. Insero, G., Fusi, F. & Romano, G. The safe use of lasers in biomedicine: Principles of laser-matter interaction. *Journal of Public Health Research*, **12**, 1-13, (2023).
2. West, G., Doughty, A., Liu, K. & Chen, W. Monitoring tissue temperature during photothermal therapy for cancer. *Journal of Bio-X Research*, **2**, 2757-2767 (2020).
3. Malcangi, G. et al. Therapeutic and adverse effects of lasers in dentistry: A systematic review. *Photonics*, **10**, 650 (2023).
4. Chernov, M. et al. Histological assessment of thermal damage in the brain following infrared neural stimulation. *Brain Stimulation*, **7**, 476-482 (2014).
5. Henderson, T. et al. Multi-watt near-infrared phototherapy for the treatment of comorbid depression: An open-label single-arm study. *Frontiers in Psychiatry*, **8**, 1-5 (2017).
6. ANSI, Z136. 1–2022. American National Standard for the Safe Use of Lasers 2022.
7. IEC, 60825-1:2014. International Standard for Safety of Laser Products 2014.
8. Landry, R., Pfefer, J. & Ilev, I. Laser and Optical Radiation Safety in Biophotonics., Chapter to the Book *Biomedical Photonics Handbook*, Ed. Tuan Vo-Dinh (CRC Press, **1**, pp. 281-309, 2014).
9. Markolf, H. Interaction Mechanisms. Chapter to the Book *Laser-Tissue Interactions: Fundamentals and Applications* (Springer-Verlag Berlin Heidelberg, Third Edition, 2007).
10. Pearce, J. Irreversible tissue thermal alterations: Skin burns, thermal damage, and cell death. Chapter to the Book *Theory and Application of Heat Transfer in Humans*, Ed. Devashish Shrivastava (John Wiley & Sons Ltd., 2018).
11. Jordan, K. et al. Impact of skin tone and cupping on erythema and thermal imaging measurements. *Scientific Reports*, **15**, 42575 (2025).
12. Ansari, M. et al., Mechanisms of laser-tissue interactions: Tissue thermal properties. *Journal of Lasers in Medical Sciences*, **4**, 99-109 (2013).
13. Shurrab, K. et al. Development of temperature distribution and light propagation model in biological tissue irradiated by 980 nm laser diode and using COMSOL simulation. *Journal of Lasers in Medical Sciences*, **8**, 118-122 (2017).
14. Dremin, V. et al. Simulation of thermal field distribution in biological tissue and cell culture media irradiated with infrared wavelengths. *Optical Express*, **20**, 23078-23089 (2022).
15. Kim, H-Y. et al. Laser–tissue interaction simulation considering skin-specific data to predict photothermal damage lesions during laser irradiation. *Journal of Computational Design and Engineering*, **10**, 947–958 (2023).

16. Tuchin, V. et al. Tissue optics and photonics: Light tissue interactions. *Journal of Biomedical Photonics and Engineering*, **2**, 030201-01-31 (2016).

17. Bergmann, F. et al. Ex vivo determination of broadband absorption and effective scattering coefficients of porcine tissue. *Photonics*. **8**, 365 (2021).

18. Hamdy, O. et al. Optical characterization of biological tissues based on fluorescence, absorption, and scattering properties. *Diagnostics*, **12**, 2846 (2022).

19. Mosca, S. et al. Optical characterization of porcine tissues from various organs in the 650-1100 nm range using time-domain diffuse spectroscopy. *Biomedical Optics Express*. 11, 1697-1706 (2020).

20. Ismail, M. et al. Absorption, thermal relaxation time, and beam penetration depth of laser wavelengths in ex vivo porcine gingival tissues. *Dentistry Journal*. **13**, 397 (2025).

21. Roibu, E. et al. Thermographic changes during soft tissue incisions with diode infrared lasers. *Photobiomodulation, Photomedicine, and Laser Surgery*, **41**, 638-643 (2023).

22. Romanos, E. et al. Effects of local anesthetics on tissue penetration using diode lasers in intraoral tissues. *Photobiomodulation, Photomedicine, and Laser Surgery*, **42**, 598-603 (2024).

23. Prahl, S. Everything I think you should know about Inverse Adding-Doubling. *Oregon Medical Laser Center, St. Vincent Hospital*, 1344, 1-74 (2011).

24. Bost, C. Heat transfer in biological tissue with thermal damage analysis. *COMSOL Blog*. November 21 (2019).

25. Frei, W. Modeling laser-material interactions with the beer-lambert law. *COMSOL Blog*. April 13 (2015).

26. De Taboada, J. Crompton, K. Koppenhoefer, S. Yushanov. Analysis of Photothermal Ablation. *COMSOL Conference Proceedings* (2019).

27. Parker, S. et al. Current concepts of laser-oral tissue interaction. *Dentistry Journal*. **8**, 61 (2020).

28. Kulkarni, U. et al. Porcine buccal mucosa as an in vitro model: Relative contribution of epithelium and connective tissue as permeability barriers. *Journal of Pharmaceutical Sciences*. **98**, 471-483 (2009).

29. Peng, M. et al. A critical review of the model fitting quality and parameter stability of equilibrium adsorption models. *Advances in Colloid and Interface Science*. **262**, 50-68 (2018).